Supplementary Information

Enhancing the Surface Lewis Basicity of Phosphorene-Hosted NiO Nanosheets for Sensitive and Selective H_2S Gas Sensing

Yahui Tian,[a] *Wenfang Zhai,*[b,c,*] *Jie Su,*[c] *Yuxin Zhao,*[d] *Zhengfei Dai,*[c] *Wei Gan,*[a,*] *and Hui Li*[a,e,*]

[a] Information Materials and Intelligent Sensing Laboratory of Anhui Province, Institutes of Physical Science and Information Technology, Anhui University, Hefei 230601 P. R. China Email: ganw@ahu.edu.cn, huili@ahu.edu.cn

[b] Materials Interface Center, Shenzhen Institute of Advanced Technology, Chinese Academy of Sciences, Shenzhen 518055, P. R. China, Email: wf.zhai@siat.ac.cn

[c] State Key Laboratory for Mechanical Behavior of Materials, Xi'an Jiaotong University, Xi'an 710049, P. R. China

[d] CNPC Tubular Goods Research Institute (TGRI), Xi'an 710077, China

[e] Leibniz International Joint Research Center of Materials Sciences of Anhui Province, Anhui University, 230301, Hefei, China

S1. Experimental section

S1.1 Chemicals

Bulk BP crystal (99%), tetrabutylammonium tetrafluoroborate (TBAB, 98%), N, N-dimethylformamide (DMF, 99.5%), nickel nitrate hexahydrate ($Ni(NO_3)_2 \cdot 6H_2O$, 99%), 2-methylimidazole (99.9%), methanol(99.9%), ethanol(99.9%) were purchased from Sinopharm.

S1.2 Preparation of BP nanosheets

Two-dimensional BP nanosheets can be prepared by electrochemical exfoliation of bulk BP. DMF solution (30 mL) dissolved with 0.3 g of TBAB was used as the electrolyte. A two-

phase DC power supply was used, with a Pt wire as the anode, and bulk BP of 30 mg as the cathode. Apply a constant voltage of 20 V for 30 min, the bulk BP crystals to swell into spongy shape. Then, the spongy BP was using a biomixer for 10 min, the spongy BP was dispersed into uniform BP nanosheets, which were centrifugally cleaned using ethanol and water for several times. Finally, the BP nanosheets were collected after drying under vacuum at 60 ˚C.

S1.3 Preparation of NiO nanosheets

NiO catalyst was prepared as follows: 290.8 mg of $Ni(NO_3)_2 \cdot 6H_2O$ was added to 20 mL methanol, which was recorded as solution A, and 328.4 mg of 2-methylimidazole was dispersed into 20 mL methanol, which was recorded as solution B. Solution A and solution B were mixed to form solution C, which was transferred to the 50 mL Teflon-lined stainless-steel autoclave and then remained under a temperature of 140 ˚C for 8 h. After cooling down to room temperature, the product was collected through centrifuging, washed with water/ethanol thoroughly, and $Ni(OH)_2$ powder was obtained after drying at 60 ˚C for 12 h. Subsequently, $Ni(OH)_2$ powder was heat-treated using a muffle furnace, and NiO powder was obtained after being kept at 300 ˚C for 1 h, which was used for the subsequent preparation of NiO/BP heterostructures.

S1.4 Preparation of NiO/BP nanosheets

$Ni(OH)_2$ nanosheets were of *in-situ* grown on the surface of 10 mg BP NSs, through a hydrothermal reaction of 29 mg of $Ni(NO_3)_2 \cdot$and 32.8 mg of 2-methylimidazole in 40 ml methanol at 140 ˚C for 8 h. The as-prepared $Ni(OH)_2$/BP nanosheets were then annealed at 300 ˚C for 1 h in argon atmosphere, forming the final NiO/BP heterostructure (NiO/BP-2). The preparation process of the NiO/BP-1 and NiO/BP-3 catalysts was similar to that of NiO/BP-2, except that 14.5 mg $Ni(NO_3)_2 \cdot$and 16.4 mg 2-methylimidazole was added for synthesis NiO/BP-1, 58 mg $Ni(NO_3)_2 \cdot$and 65.6 mg 2-methylimidazole was added for synthesis NiO/BP-3.

S1.5 Characterizations

Field emission scanning electron microscope (FESEM, FEI Verios460) and transmission electron microscope (TEM, JEM-2100F) with high resolution TEM (HRTEM) images, selected area electron diffraction (SAED) patterns, energy dispersive X-ray spectrometer (EDS) elemental mapping were adopted to observe the morphologies. X-ray

diffraction (XRD, PANalytical X'Pert Pro) with filtered Cu Kα radiation (λ= 1.54056 Å) was used to detect the sample's crystalline structures. X-ray photoelectron spectroscopy (XPS, Thermo Fisher Scientific ESCALAB Xi+) was obtained the electronic states and the elemental composition near the catalyst surface. Fitting analysis of XPS data using XPSPEAK41 software. Raman spectra was probed using Horiba HR800 spectrometer with excitation source of 532 nm laser. The functional groups on the samples were investigated by Fourier transform infrared spectrometer (FTIR, IRPrestige-21).

S1.6 Gas sensing measurements

Au interdigital electrodes (200 μm spacing, 200 μm width, 8 pairs with a microheater underneath) were employed to test the gas sensing performance of samples. Pt wire was linked with such an electrode to build a sensor. Firstly, 30 mg powder sample was uniformly dispersed in 1 mL ethanol under ultra-sonication. And then 2 μL dispersed sensing materials were dropped on the electrode with a pipette and dried naturally. At last, the gas sensing performance were tested using a dynamical gas sensing system (Fig. S10). The gas concentrations were controlled by adjusting the flow rate of of target gas and dry air, keeping a constant flow rate of gas mixture as 500 sccm. A Keithley DMM6500 multimeter was employed to record the resistance variations of sensors during gas sensing experiments.

S1.7 Electrochemical test

The catalytic ink is prepared by dispersing 5 mg samples in a mixture of 0.9 mL ethanol, 0.08 mL ultrapure water and 0.02 mL Nafion. Afterward, 5 μL ink was placed uniformly on a glass-carbon (GC) electrode (3 mm diameter) and dried slowly. The double-layer capacitance (C_{dl}) of samples was examined using Autolab PGSTAT204 station with a conventional 3-electrode set-up in 1 M KOH. And the C_{dl} measurements within the range of 1.07-1.17 V vs. RHE were detected with scan speed from 20 mV s^{-1} to 100 mV s^{-1}, respectively. C_{dl} was calculated by plotting the half of current density difference between positive and negative scan (Δj) at 1.12 V vs. RHE against the scan rates.

S1.8 DFT calculations

Density function theory (DFT) was used to study the electronic structure of all samples. The DFT calculations were carried out based on projector augmented-wave (PAW) method and the Vienna Ab Initio Simulation Package (VASP) code, employing Perdew-Burke-Ernzerhof

(PBE) and generalized gradient approximation (GGA).[S1]The van der Waals (vdW) interaction was described by using an empirical correction DFT-D3 method. Black phosphorus (0 2 0) was used k-points grid of 3×3×1 and 6×6×1 for structure optimization and density of states (DOS) calculations, respectively. The cutoff energy was 450 eV and the convergence of energy and forces were 10^{-5} eV and 0.01 eV $Å^{-1}$. To evaluate the stability of gas absorption on the sensing materials, the absorption energy (E^*_{ads}) was calculated using Equation (1).

$$E_{*ads} = E_{*(sub+gas)} - E_{*sub} - E_{*gas} \qquad (1)$$

where the E_{*gas} is the energy of the baregas, E_{*sub} is the energy of the substrate (sensing materials), and $E_{*(sub+gas)}$ is the total energy of the adsorbed gas molecule system.[S2]

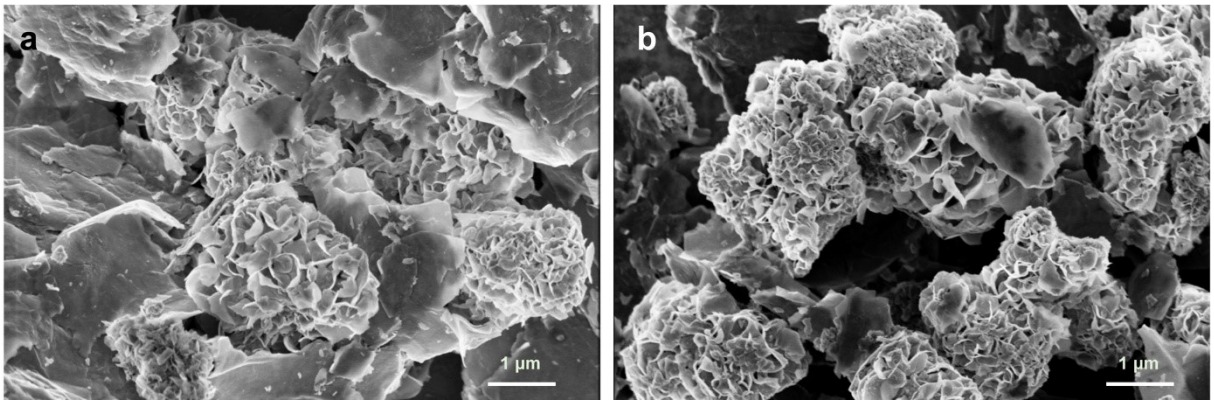

Fig. S1. SEM images of (a) NiO/BP-1 and (b) NiO/BP-1 composite materials.

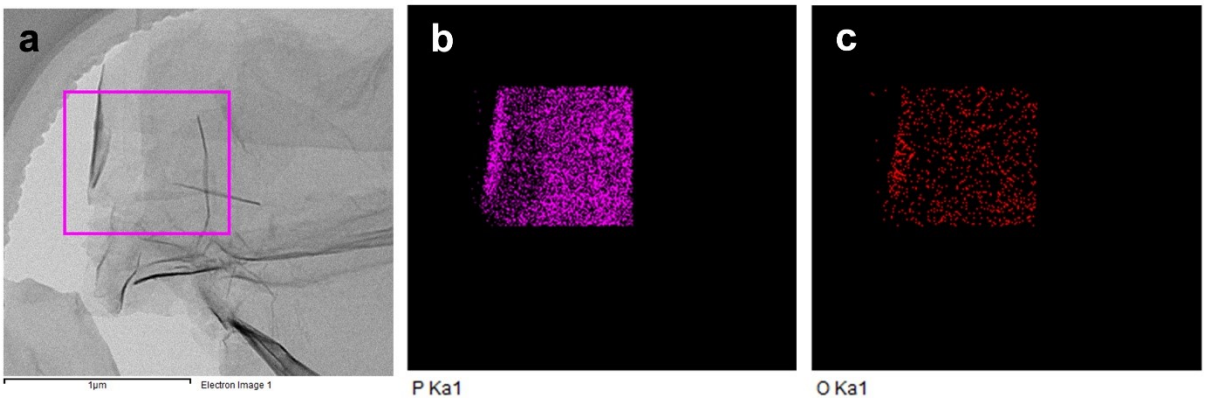

Fig. S2. (a) TEM and (b-c) elemental mapping images of BP NSs.

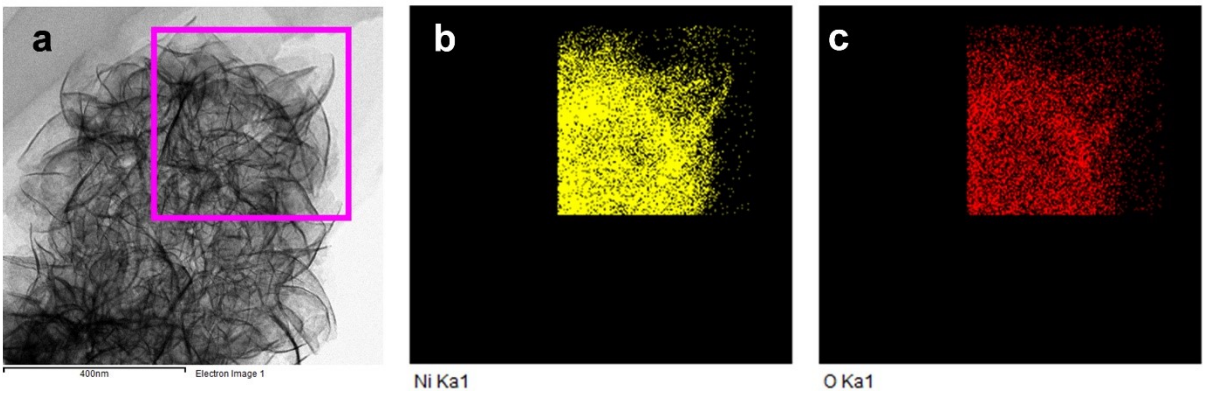

Fig. S3. (a) TEM and (b-c) elemental mapping images of NiO NSs.

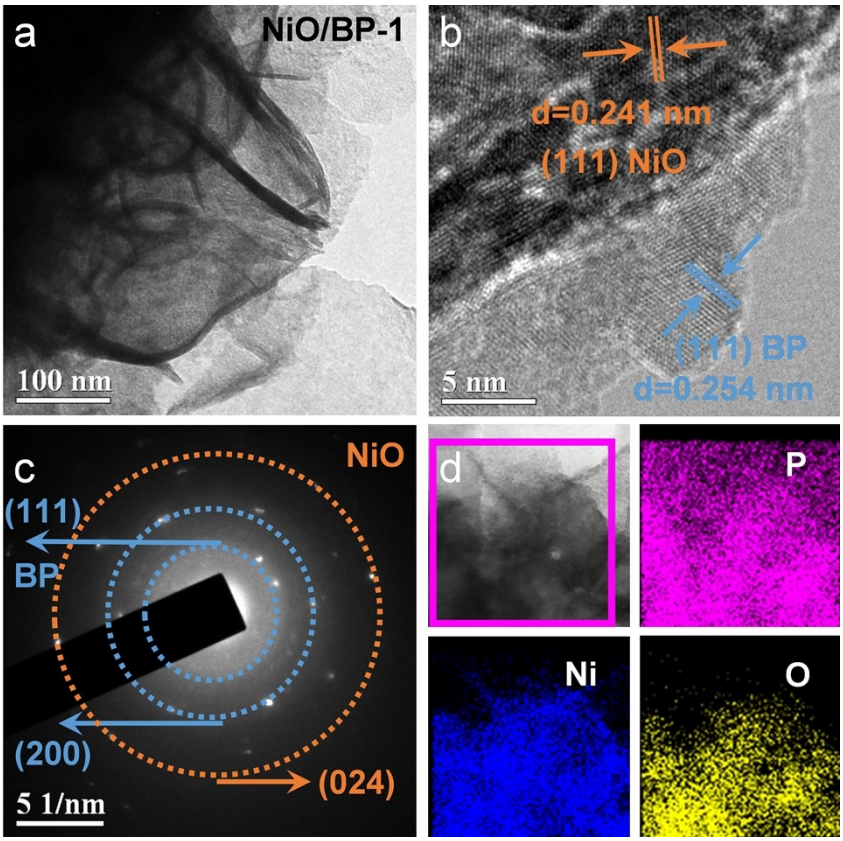

Fig. S4. (a) TEM image, (b) HRTEM image, (c) SAED pattern, and (d) elemental mapping images of NiO/BP-1 heterostructure.

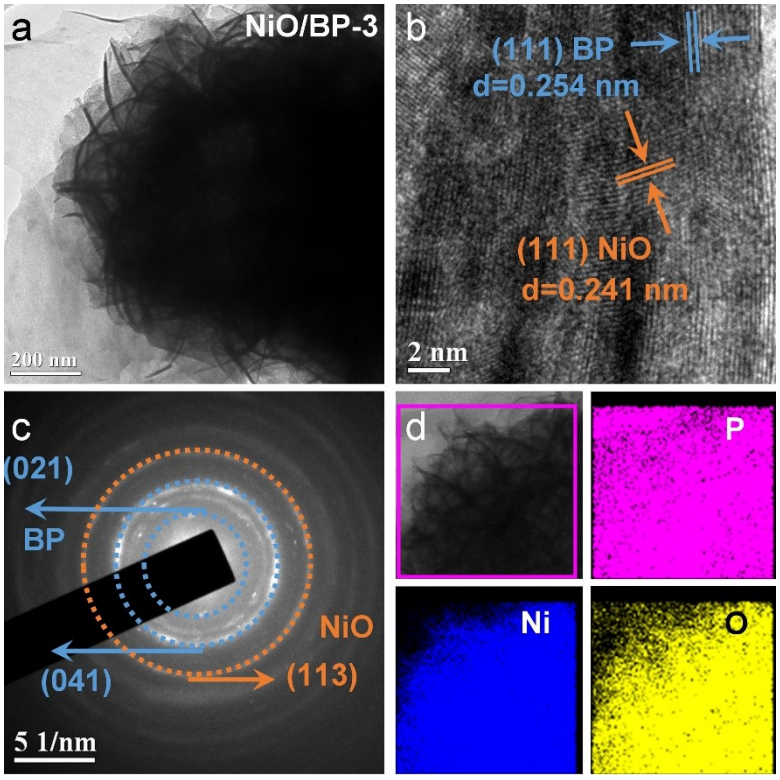

Fig. S5. (a) TEM image, (b) HRTEM image, (c) SAED pattern, and (d) elemental mapping images of NiO/BP-3 heterostructure.

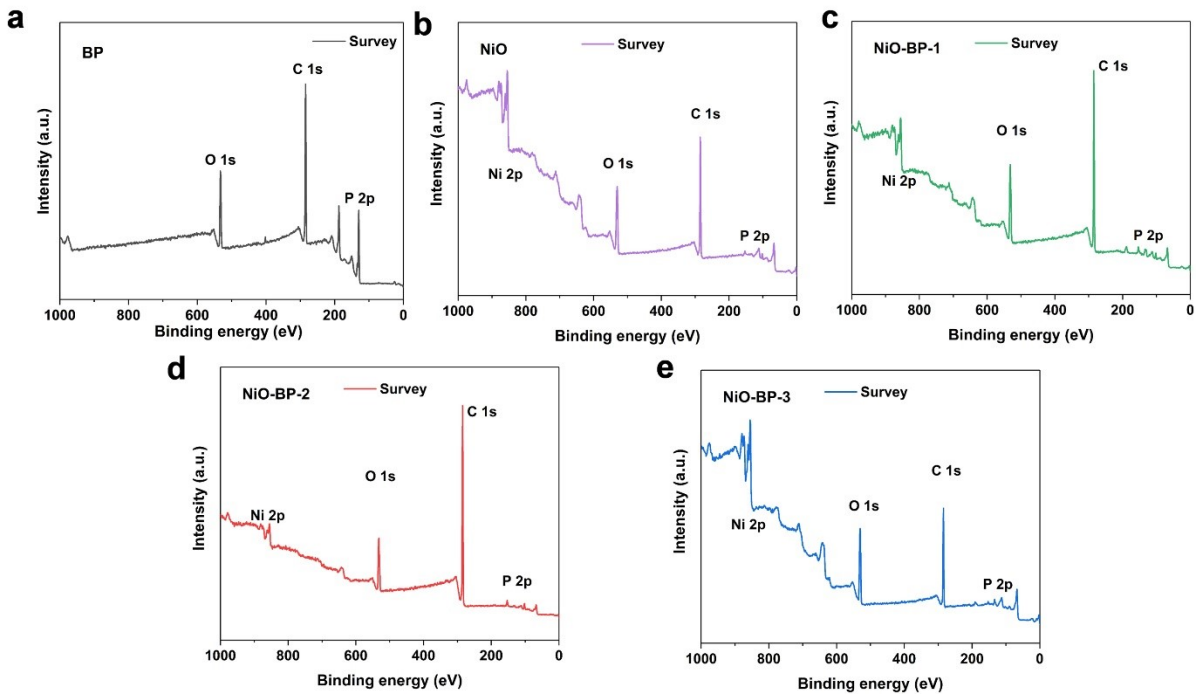

Fig. S6. XPS survey spectra of (a) BP NSs, (b) NiO NSs, (c) NiO/BP-1, (d) NiO/BP-2, and (e) NiO/BP-3 samples.

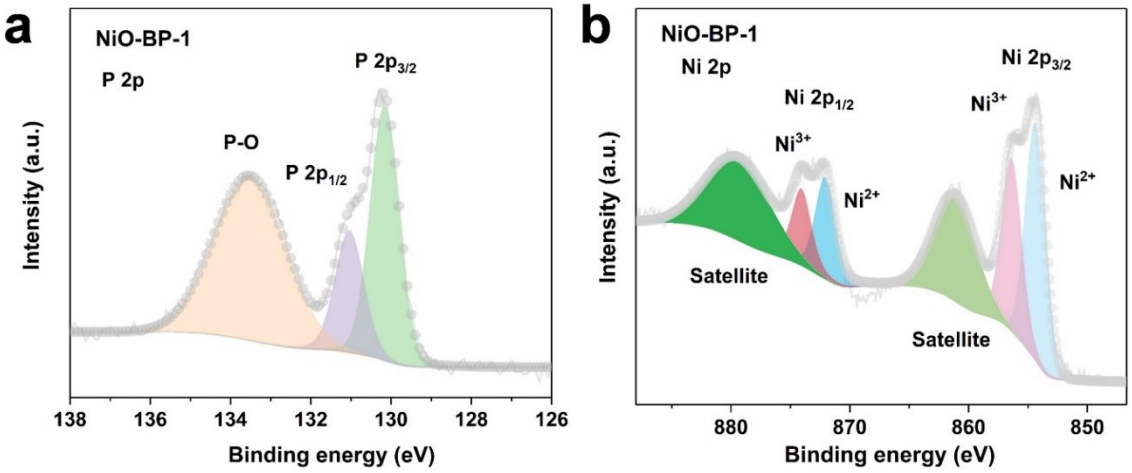

Fig. S7. XPS spectra of NiO/BP-1. (a) P 2p, (b) Ni 2p.

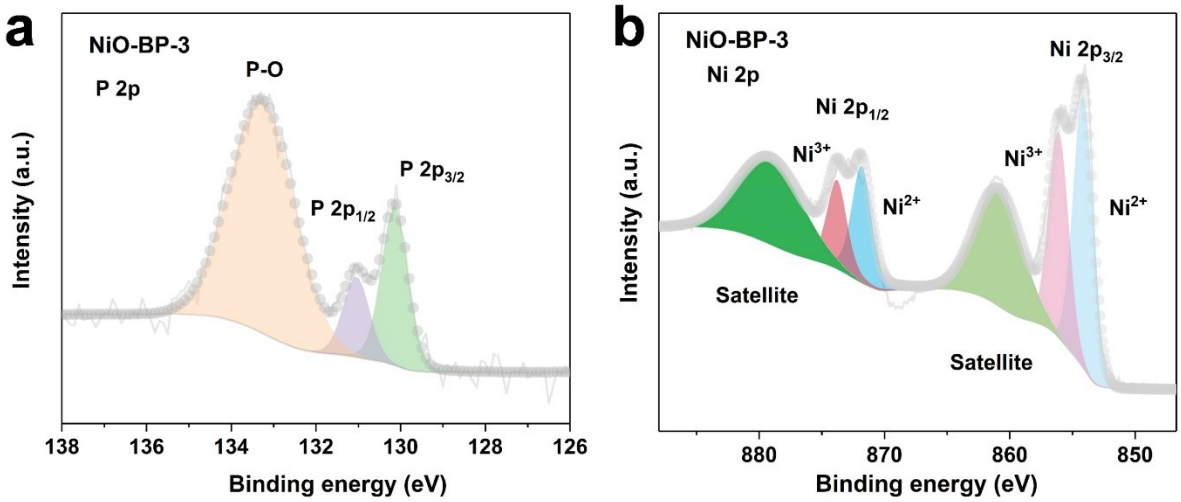

Fig. S8. XPS spectra of NiO/BP-3. (a) P 2p, (b) Ni 2p.

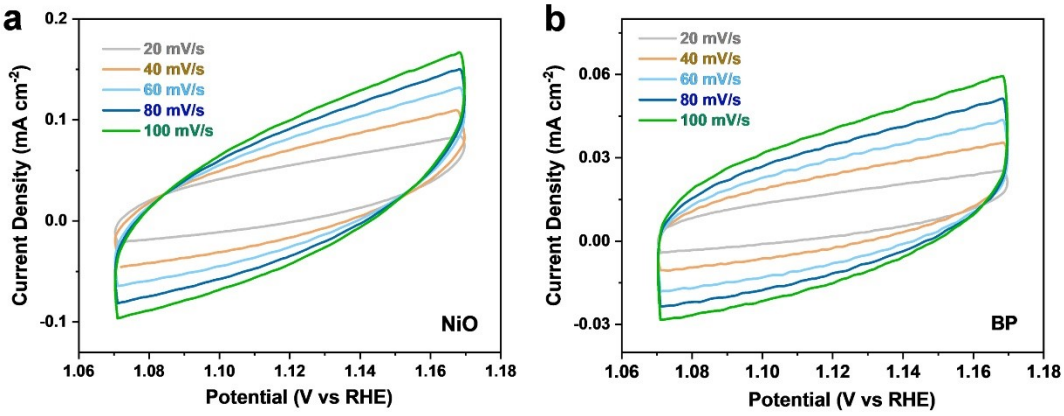

Fig. S9. CV curves at different scan rates in non-faradaic region for (a) NiO and (b) BP.

In this work, we have tested the C_{dl} in 1 M KOH within the range of 1.07-1.17 V vs. RHE, which is always used for the C_{dl} measurement in electron-donating oxygen evolution reaction (OER, $4OH^- \rightarrow O_2+2H_2O+4e^-$). The larger C_{dl} corresponds the higher OER activity and the stronger electron donating behavior. In this regard, the higher C_{dl} of NiO/BP heterostructure (Fig. 4f) suggests the stronger electron donating character and higher surface basicity.

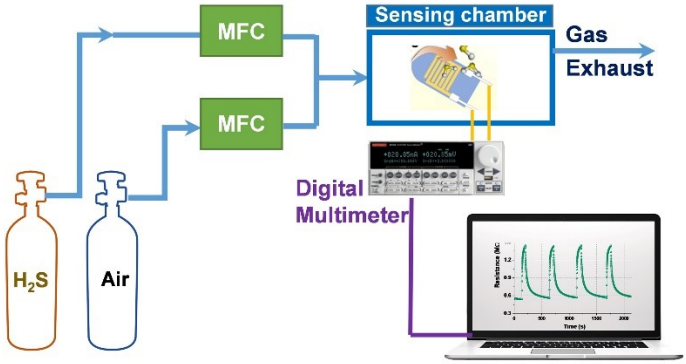

Fig. S10. Schematic description of the gas-sensing installation.

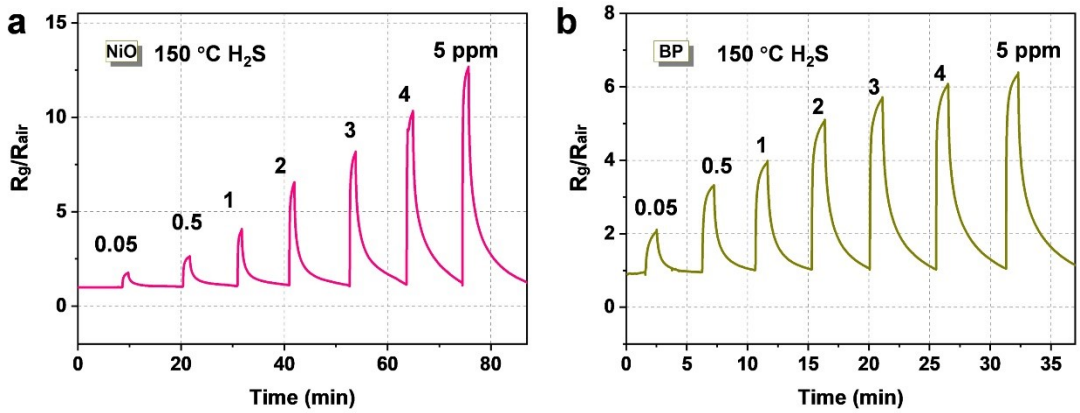

Fig. S11. The dynamic sensing transients to 0.05 – 5 ppm H_2S of (a) NiO and (b) BP-based sensors at 150 ºC.

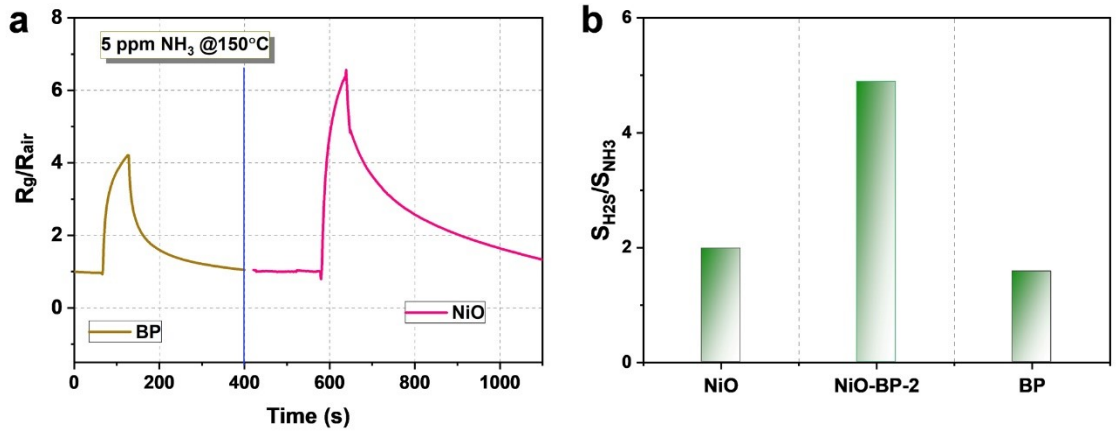

Fig. S12. (a) The sensing transients to 5 ppm H_2S and 5 ppm NH_3 at 150 ºC. (b) Bar graph summarizing the H_2S/NH_3 selectivity for different sensors at 150 ºC.

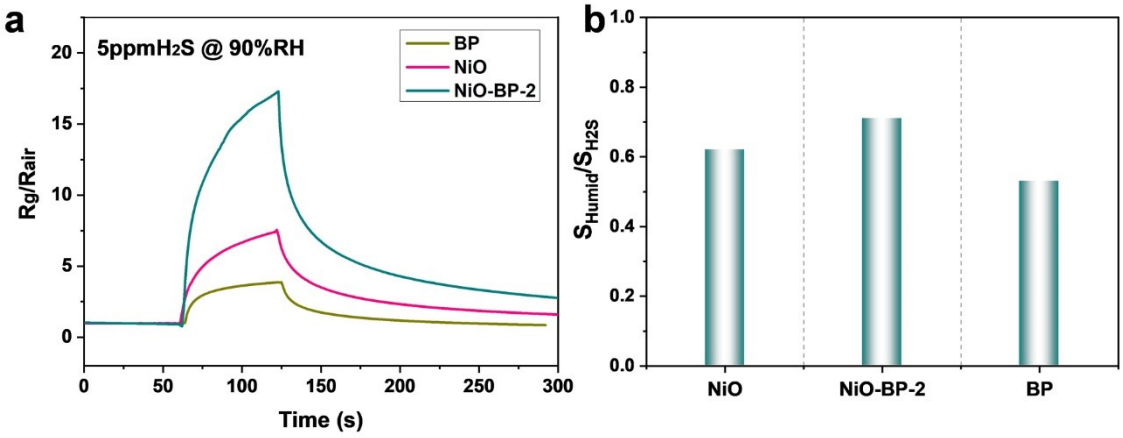

Fig. S13. (a) The sensing response curves of BP, NiO, and NiO/BP-2 based sensors to 5 ppm H_2S at 150 ºC and 90%RH. (b) Bar graph summarizing the response value ratio (90%RH H_2S (S_{Humid}) to dry H_2S (S_{H2S})) for different sensors at 150 ºC. The higher S_{Humid}/S_{H2S} ratio of NiO/BP-2 suggests the better anti-humidity influence sensor performance.

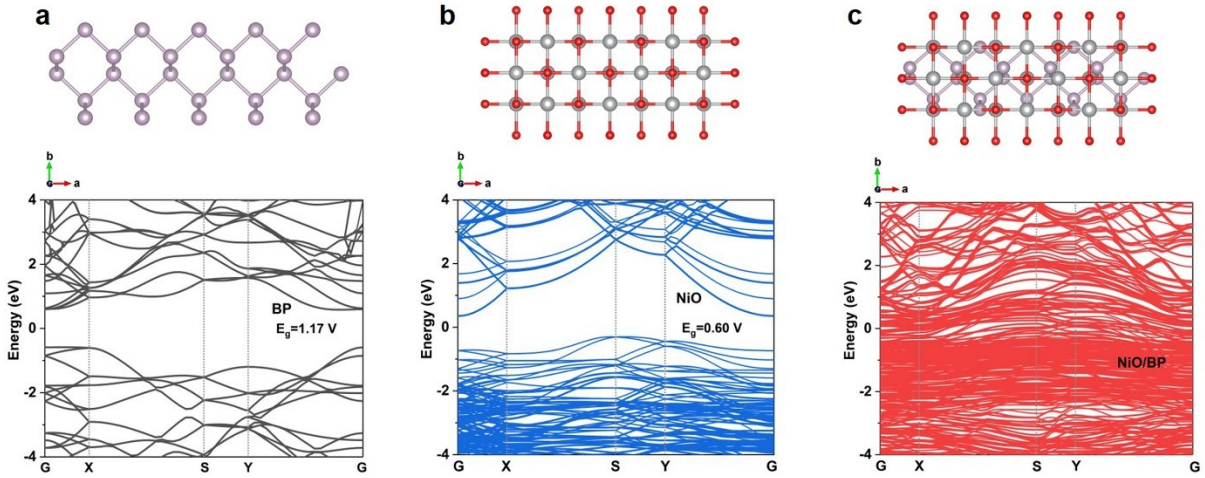

Fig. S14. Band structures of (a) BP, (b) NiO, and (c) NiO/BP, respectively.

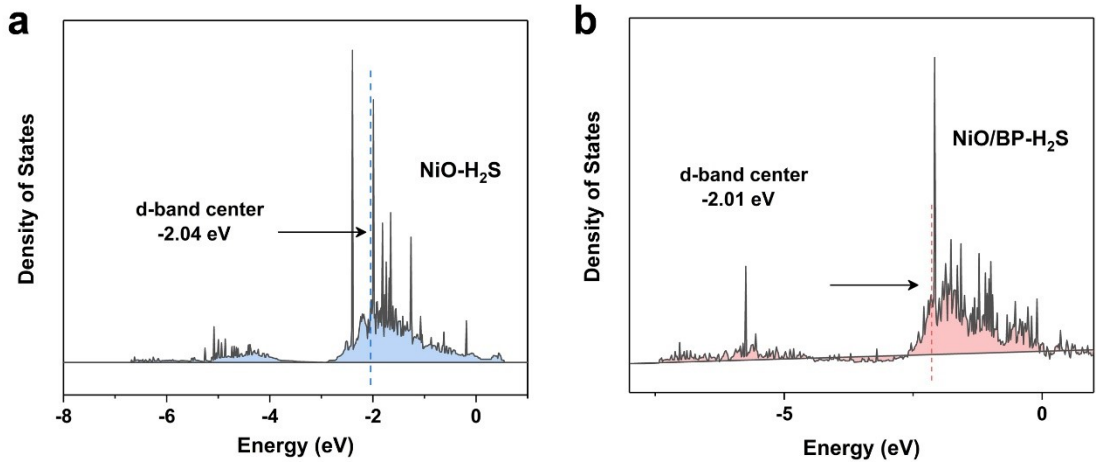

Fig. S15. d-band center configurations of (a) NiO and (b) NiO/BP after H_2S adsorption.

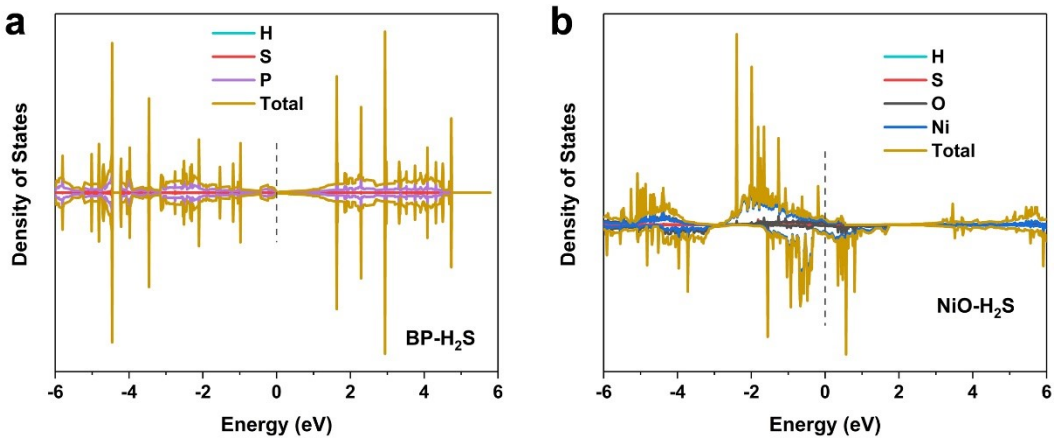

Fig. S16. DOS of (a) BP and (b) NiO after H_2S adsorption.

Table S1. Comparison of sensing performance based on BP or Ni-based nanomaterials towards H_2S in the previous literatures.

Sensing materials	Working Temperature	Gas concentration	Response Rg/Ra	Detection limit	Ref.
NiO/BP-2	**150 ºC**	**5 ppm**	**24.3**	**0.05 ppm**	**This work**
SnO_2/BP	130 ºC	5 ppm	10	1 ppm	[S3]
BP-WO_3	190 ºC	5 ppm	1.4	0.3 ppm	[S4]
Defective NiO	150 ºC	5 ppm	9	1 ppm	[S5]
ZnO–NiO	250 °C	5 ppm	1.5	1 ppm	[S6]
Ni-WO_3	250 °C	10 ppm	17	2.5 ppm	[S7]
Co_3O_4@NiO	200 °C	20 ppm	48	20 ppm	[S8]
Co_3O_4/$NiCo_2O_4$	200 °C	50 ppm	57	10 ppm	[S9]
6% Zn-NiO	270 °C	10 ppm	6.1	0.05 ppm	[S10]

Reference

[S1] J. Perdew, K. Burke, and M. Ernzerhof. *Phys Rev Lett* 1996; **77**, 3865-3868.

[S2] T. Liang, Z. Dai, Y. Liu, X. Zhang and H. Zeng, *Sci. Bull.*, 2021, **66**, 2471-2478.

[S3] Y. Zhou, Z. Hu, H. Zhao, Y. Wang, J. Li and C. Zou, *Anal. Chim. Acta*, 2023, **1245**, 340825.

[S4] C. Zheng, Y. Shi, B. Tang and J. Zhang, *Sensors*, 2024, **24**, 1376.

[S5] K. Li, Y. Luo, B. Liu, H. Wang, L. Gao and G. Duan, *Chem. Eng. J.*, 2022, **432**, 134302.

[S6] J. N. O. Amu-Darko, S. Hussain, E. Issaka, M. Wang, A. A. Alothman, S. Lei, G. Qiao and G. Liu, *Ceram. Int.*, 2024, **50**, 17681-17690.

[S7] H. T. T. Nguyen, T. H. Truong, T. D. Nguyen, V. T. Dang, T. V. Vu, S. T. Nguyen, X. P. Cu and T. T. O. Nguyen, *J. Mater. Sci.* 2020, **31**, 12783-12795.

[S8] X. Wang, J. Lu, W. Han, J. Yang, B. Jiang, Y. Sun, H. Zhang and G. Lu, *Sens. Actuator B-Chem*, 2021, **342**, 130028.

[S9] J. Tan, S. Hussain, C. Ge, M. Wang, S. Shah, G. Liu and G. Qiao, *Sens. Actuator B-Chem*, 2020, **303**, 127251.

[S10] O. Wang, J. Kong, Z. Xue, B. An, J. Xu and X. Wang, *ACS Sens.* 2024, **9**, 3233-3243.